Comparison of the Distorted Born Iterative and Multiplicative-Regularized Contrast Source Inversion methods: the 2D TM case

Colin Gilmore, Puyan Mojabi, and Joe LoVetri

University of Manitoba
R3T 5V6, Canada
cgilmore@ee.umanitoba.ca, pmojabi@ee.umanitoba.ca, lovetri@ee.umanitoba.ca

Abstract: For 2D Transverse Magnetic (TM) microwave inversion, we compare the Distorted Born Iterative Method (DBIM) and the Multiplicative-Regularized Contrast Source Inversion (MR-CSI) based on two sets of experimentally collected measurement data. The regularization parameter associated with the DBIM is selected automatically using a fast *L*-curve method which makes possible a direct comparison between the two methods. The results show that the MR-CSI method out-performs the DBIM in the cases considered herein.

Keywords: Microwave inversion, multiplicative-regularized contrast source inversion, distorted born iterative method, regularization.

1. Introduction

The microwave inverse scattering problem has been an area of interest for many years and research into this field has led to the development of a multiplicity of inversion algorithms. In this paper we consider and compare two well-known inversion techniques: Multiplicative Regularized-Contrast Source Inversion (MR-CSI) [1,2] and the Distorted Born Iterative Method (DBIM) [3], which are applied to 2D Transverse Magnetic (TM) inverse problem. These two methods both cast the inverse problem as an optimization problem, but differ significantly in the objective function which is to be minimized, the minimization procedures, and the methods for regularizing inherent ill-posedness of the inverse scattering problem.

This comparison is made possible by recent advances in regularization parameter choice methods. While the MR-CSI method automatically adjusts the regularization without any user input, the DBIM (and other inversion techniques such as the gradient method) rely on the selection of a regularization parameter which is typically determined through considerable numerical experimentation, or *a-priori* knowledge of the noise level of the measured data. However, with our use of an automatic parameter choice method, the regularization parameter in DBIM is automatically set to the optimal value (in the sense of the *L*-curve method [5,6]) without user input or advance knowledge of the noise level. The use of an automatic parameter choice method for the DBIM eliminates the uncertainty and lack of reproducible results which would otherwise complicate a direct comparison between these two techniques.

2. MR-CSI Method

The many advantages of this inversion technique include that it does not require any *a-priori* information (but it may easily be taken into account if desired), no forward solver is required in the optimization procedure, and it has a computational complexity of only approximately twice that of a

forward solver. In addition, the regularization parameter for the MR is selected by the algorithm itself without significantly increasing the computational complexity.

The data equation is first re-written as:

$$f_k(\boldsymbol{r}) = k_b^2 \int_D g(\boldsymbol{r}, \boldsymbol{r}')\chi(\boldsymbol{r}')u_k(\boldsymbol{r}')d\boldsymbol{r}' \qquad \boldsymbol{r} \notin D, \tag{1}$$

where f_k is the measured data. It is assumed that (1) does not hold exactly, as the data are unavoidably corrupted with noise. In symbolic notation, we now write the data equation as

$$f_k = G^S \chi u_k \tag{2}$$

where the operator G^S is defined as

$$G^S[*] \equiv k_b^2 \int_D g(\boldsymbol{r}, \boldsymbol{r}')[*]d\boldsymbol{r}' \qquad \boldsymbol{r} \in S, \tag{3}$$

and S is a measurement surface (or set of discrete measurement points). Similarly, the domain equation is written as

$$u_k = u_k^{inc} + G^D \chi u_k \tag{4}$$

where the operator G^D is defined as

$$G^D[*] = k_b^2 \int_D g(\boldsymbol{r}, \boldsymbol{r}')[*]d\boldsymbol{r}' \qquad \boldsymbol{r} \in D. \tag{5}$$

Next, define the *contrast sources*, $w_k(\boldsymbol{r})$ as

$$w_k(\boldsymbol{r}) = \chi(\boldsymbol{r})u_k(\boldsymbol{r}) \qquad \boldsymbol{r} \in D. \tag{6}$$

By multiplying both sides of the domain equation, (4) with the contrast, χ, and utilizing the definition of the contrast sources we may write

$$\chi u_k^{inc} = w_k - \chi G^D w_k \qquad \boldsymbol{r} \in D. \tag{7}$$

The CSI method formulates the inverse problem as an optimization function in two variables: the contrast, χ and the contrast sources, w. The objective function is minimized via an iterative optimization scheme. The core of the CSI method is the objective function

$$F_n = F(w_{k,n}, \chi_n) = F^S(w_{k,n}) + F^D(w_{k,n}, \chi_n), \tag{8}$$

where each term on the right hand side is created by summing over the transmitter index, k:

$$F^S(w_{k,n}) = \frac{\sum_k \|\rho_{k,n}\|_S^2}{\sum_k \|f_k\|_S^2} \text{ and } F^D(w_{k,n}, \chi_n) = \frac{\sum_k \|r_{k,n}\|_D^2}{\sum_k \|\chi_n u_k^{inc}\|_D^2}. \tag{9}$$

Here ρ is the data error, defined as

$$\rho_{k,n}(\boldsymbol{r}) = f_k(\boldsymbol{r}) - G^S w_{k,n} \qquad \boldsymbol{r} \in S, \tag{10}$$

and $r_{k,n}$, known as the domain (or object) error, is defined as

$$r_{k,n}(\boldsymbol{r}) = \chi_n u_{k,n} - w_{k,n} = \chi G^D w_k + \chi u_k^{inc} - w_{k,n} \qquad \boldsymbol{r} \in D. \tag{11}$$

The index $n = 1 \ldots N$ represents the iteration number. The normalization terms in both F^S and F^D (9) are utilized to balance between the two terms in the overall objective function.

An important aspect of the CSI method is the inclusion of the domain equation inside the objective function thus obviating the need for a separate forward solver. The minimization over both unknowns χ and w_k is performed sequentially by taking alternating steps of the conjugate gradient minimization algorithm on each unknown. Closed-form expressions used in this minimization algorithm are available, which significantly increases the computational efficiency. The details of the minimization can be found in [1,2].

3. Multiplicative Regularization

The CSI method may be further enhanced via the use of Multiplicative Regularization (MR) which is based on minimizing the total variation of the contrast. The MR-CSI objective function becomes

$$C = F_{MR}(\chi_n) F_n(w_{k,n}, \chi_n) \tag{12}$$

where

$$F_{MR}(\chi_n) = \frac{1}{A}\int_D \frac{|\nabla \chi_n(\boldsymbol{r})|^2 + \delta_n^2}{|\nabla \chi_{n-1}(\boldsymbol{r})|^2 + \delta_{n-1}^2} d\boldsymbol{r} \tag{13}$$

where A is the area of the imaging region D, $\delta_{n-1}^2 = F_{n-1}^D \Delta^{-2}$, and Δ is the length of a side of single cell in the discretized domain (*i.e.* Δ^{-2} represents the reciprocal of the area of a single cell area of the domain D. For example, on a rectangular grid $\Delta^{-2} = 1/(\Delta x \Delta y)$).

In all cases considered in this paper, we utilize the multiplicative regularized version of the CSI algorithm.

4. The Distorted Born Iterative Method with Additive Tikhonov Regularization

The Distorted Born Iterative Method (DBIM) is based on the minimization of the norm:

$$\underset{\chi_n}{\operatorname{argmin}} \sum_k \left\| f_k - G^S \chi_n u_{k,n} \right\|_S^2 \text{ subject to } (I - G^D \chi_n) u_{k,n} = u_k^{inc} \tag{14}$$

where I is the identity operator. Minimizing this norm minimizes the discrepancy between the measured scattered field and the simulated scattered field computed at the receiver points through a forward solver.

As can be seen, (14) is a nonlinear functional in terms of χ_n:

$$\sum_k \left\| f_k - G^S \chi_n (I - G^D \chi_n)^{-1} u_k^{inc} \right\|_S^2. \tag{15}$$

The DBIM casts this nonlinear optimization problem into a linearized optimization problem. First, the $(I - G^D \chi_n)^{-1}$ operator is approximated by I (the well-known Born approximation). This linearized problem is inherently ill-posed and is treated here using additive regularizers which will be discussed in the next section.

Next, assuming χ_n is known (n starts at 1; so χ_1 is the contrast obtained via the Born Approximation), a distorted numerical Green's function for the new background χ_n, given by $g_n(\boldsymbol{r}, \boldsymbol{r}') = (I - G^D \chi_n)^{-1} g$ is constructed. This leads to the new data operator [4]:

$$G_n^S[*] = k_{b,n}^2 \int_D g_n(\boldsymbol{r}, \boldsymbol{r}')[*] d\boldsymbol{r}' \qquad \boldsymbol{r} \in S \tag{16}$$

where $k_{b,n}$ is the wavenumber with respect to the distorted embedding χ_n. Next, the new contrast is obtained by solving the ill-posed linearized problem:

$$\chi_{n+1} = \chi_n + \delta\chi \text{ , where } \delta\chi = \text{argmin}\left\{ F(\delta\chi;\chi_n) = \sum_k \left\| f_k - G^S \chi_n u_{k,n} - G_n^S \delta\chi u_{k,n} \right\|_S^2 \right\}. \quad (17)$$

This process is repeated until the objective function (14) is minimized to a desired level.

5. Additive Regularization for the Ill-posed Operator.

The linearized optimization problem in (17) is ill-posed as the objective function contains a Fredholm integral equation of the first kind with G_n^S as the integral operator. There are some different approaches to stabilize the problem associated with (17), but here we use Tikhonov regularization (additive regularization) which minimizes the cost functional:

$$\delta\chi = \underset{\delta\chi}{\text{argmin}}\{ F(\delta\chi;\chi_n) + \lambda^2 F^R(\delta\chi) \} \quad (18)$$

where $F^R(\delta\chi)$ is an additive regularizer and λ is the regularization parameter. Here, we choose $F^R(\delta\chi)$ as:

$$F^R(\delta\chi) = \int |\delta\chi(\boldsymbol{r}')|^2 d\boldsymbol{r}' \quad (19)$$

which is the *L2*-norm $\|\delta\chi\|_D^2$.

In this case, the null-space of the additive regularizer intersects trivially with the null-space of the ill-posed operator ensuring a unique solution for the minimization. The regularization parameter is chosen using a computationally efficient form of the *L*-curve method. Constructing the standard *L*-curve in a naive way requires the (generalized) singular value decomposition, which is computationally very expensive ($O(n^3)$). However, in this paper, the *L*-curve is constructed using Lanczos bidiagonalization which does not need singular value decomposition [6]. In this technique, the ill-posed matrix is only utilized via matrix-vector multiplication making the *L*-curve method feasible for large-scale inverse problems. The details of the use of *L*-curve for regularization parameter selection and the use of Lanczos bidiagonalization are not presented here, but are available in [5,6]. The algorithm selects the optimial regularization parameter in the sense of the *L*-curve (which corresponds to the 'corner' of the *L*-curve).

6. Results

Both inversion algorithms were run on the UPC Barcelona human forearm [8] (data set BRAGREG). In both cases, the results were restricted to lie within $0 < Real(\varepsilon_r) < 80$ and $-20 < Imag(\varepsilon_r) < 0$. The data were collected at a frequency of 2.33 GHz in an experimental microwave tomography system with a human forearm in the data collection tank, filled with a background solution of permittivity $\varepsilon_b = 77.3 - j8.66$. The inversion results for the MR-CSI and DBIM are shown in Fig. 1. The expected relative permittivities at this frequency are approximately $54 - j13$ for muscle, $38.5 - j10$ for skin, $8 - j1$ for bone marrow, and $5.5 - j0.6$ for bone.

In this case, the MR-CSI method out-performs the DBIM method. In both cases, the overall structure of the arm may be seen in the real part of the reconstructions. However, the imaginary part of the reconstruction for the DBIM method does not reconstruct anything meaningful. The one advantage of the DBIM method is that it reaches closer to the expected value for the real part of the permittivity of the bones.

For the next comparison, we utilized the *FoamTwinDielTM* data from the Fresnel data set, freely provided by Institut Fresnel to the inverse methods community [7]. The data were collected from 2 - 10 GHz with 18 transmitters and 241 receivers. The scatterer consists of a cylinder of diameter 31 mm, with contrast

~2, inside a cylinder of diameter 80 mm with contrast ~0.45. In addition, there is another external cylinder butted against the first, with diameter 31 mm, and contrast of ~2. The data at a single frequency of 2 GHz were inverted with each method. The results are shown in Fig. 2, (a) and (b). In addition, we simultaneously inverted the full multi-frequency data using both methods. The results for the MR-CSI inversion are shown Fig. 2, (c). The DBIM method did not provide a meaningful result in the simultaneous multi-frequency case and it is not shown. The results for the single-frequency case are very similar, although the DBIM overshoots the target value of 2 for the smaller cylinders. We surmise that the DBIM method does not provide a meaningful result in the multi-frequency case because the initial guess (which requires the Born approximation) is not acceptable when the object is electrically large. If the frequencies are restricted to 2-6 GHz, the DBIM reconstruction does provide meaningful results (not shown) which are not as good as the MR-CSI results for the same frequency range.

7. Discussion and Conclusion

In the cases considered here, the MR-CSI method out-performs the DBIM. We do note that the examples presented herein are far from exhaustive, and this paper does not constitute a proof of the superiority of MR-CSI. However, the DBIM is combined with an automatic regularization parameter choice method for additive regularization that ensures the optimal choice of the regularization parameter (in the sense of the *L*-curve). This removes the possibility that a better regularization parameter may be found, and thus represents the best that the DBIM with Tikhonov regularization and the *L*-curve parameter selection can do.

We speculate that the MR-CSI method out-performs the DBIM due to the presence of the Multiplicative Regularizer (MR). This conclusion is supported by the published results of the CSI method without MR [9], which show results that are very similar to the DBIM results presented herein (for the forearm data). From this observation, it seems that the use of the domain equation in the MR-CSI functional F^D (9) provides comparable results to additive (Tikhonov) regularization applied to the DBIM functional (17). It is expected that the addition of an MR term to the DBIM functional will reduce the discrepancies between these two methods. Finally, we note that the use of $\|\delta\chi\|$ as the additive regularizer in DBIM may be changed to other forms (such as total-variation), which improve the results. However, the process of selecting a regularization parameter becomes extremely computationally expensive, limiting the effectiveness of the DBIM with these other forms of additive regularization.

8. References

[1] P.M. van den Berg, and R. Kleinman, "A contrast source inversion method", *Inverse Problems*, vol. 13, pp.1607-1620, 1997.

[2] A. Abubakar, P.M. van den Berg, and J.J. Mallorqui, "Imaging of biomedical data using a multiplicative regularized contrast source inversion method," *IEEE Transactions on Microwave Theory and Techniques*, vol. 50, 2002.

[3] W.C. Chew and Y.M. Wang, "Reconstruction of two-dimensional permittivity distribution using the distorted Born iterative method". *IEEE Transactions on Medical Imaging*, vol. 9, 1990.

[4] R.F. Remis, P.M. van den Berg, "On the equivalence of the Newton-Kantorovich and distorted Born methods", *Inverse Problems*, vol. 16, 2000.

[5] P.C. Hansen and D.P. O'Leary, "The use of the *L*-curve in the regularization of discrete ill-posed problems", *SIAM Journal of Scientific computing*, vol. 14, pp 1487-1503, 1993.

[6] D. Calvetti, P.C. Hansen and L. Reichel, "*L*-curve curvature bounds via Lanczos bi-diagonalization", *Electronic Transactions on Numerical Analysis*, vol. 14, pp. 20-35, 2002.

[7] J.M. Geffrin, P. Sabouroux, and C. Eyraud, "Free space experimental scattering database continuation:

experimental set-up and measurement precision", *Inverse Problems* vol. 21, 2005.

[8] J.J. Mallorqui, N. Joachimowicz., J.Ch. Bolomey, and A.P. Broquetas, "Database of "In Vivo" Measurements for Quantitative Microwave imaging and Reconstruction Algorithms Available", *IEEE Antennas and Propagation magazine*, vol. 37, no. 5., pp. 87-89, 1995.

[9] A. Abubakar, P.M. van den Berg, and S.Y. Semenov, "Two-and three dimensional algorithms for microwave imaging and inverse scattering", *J. of Electromag. Waves and Appl*., vol. 17, 2003.

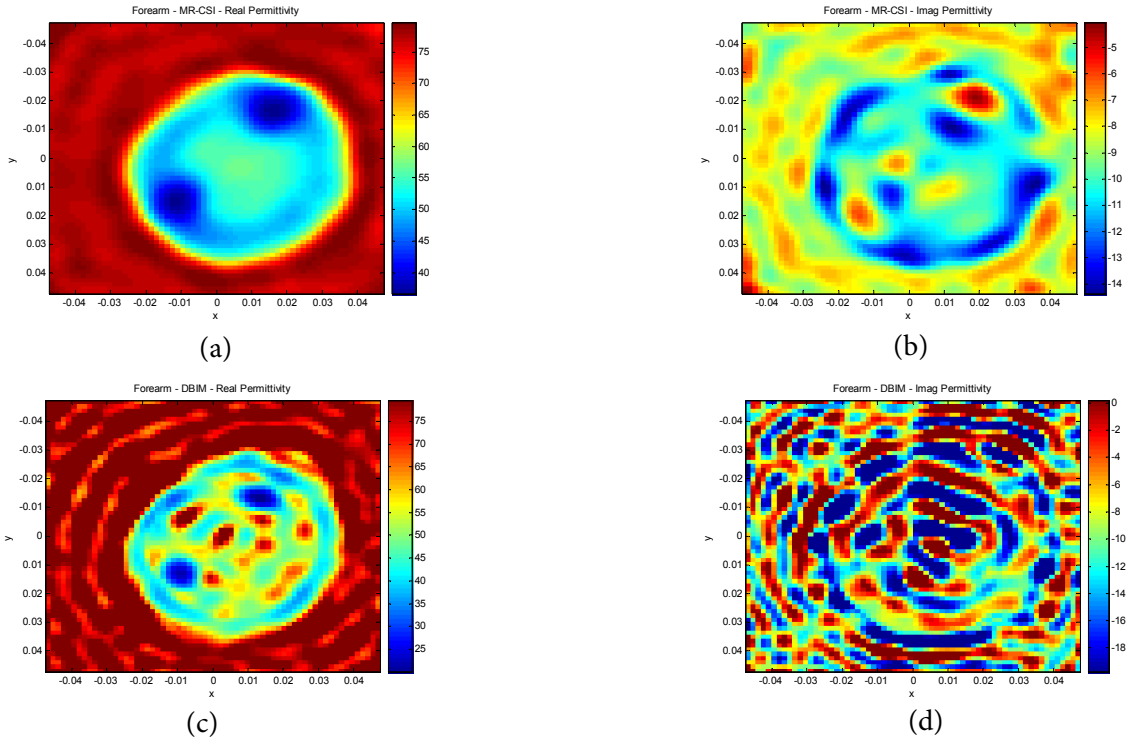

Fig. 1. Human forearm inversions: (a) real and (b) imaginary permittivities for the MR-CSI method after 1024 iterations. (c) real and (d) imaginary permittivities for the DBIM method after 9 iterations. Note that the structure of the forearm is not visible in (d).

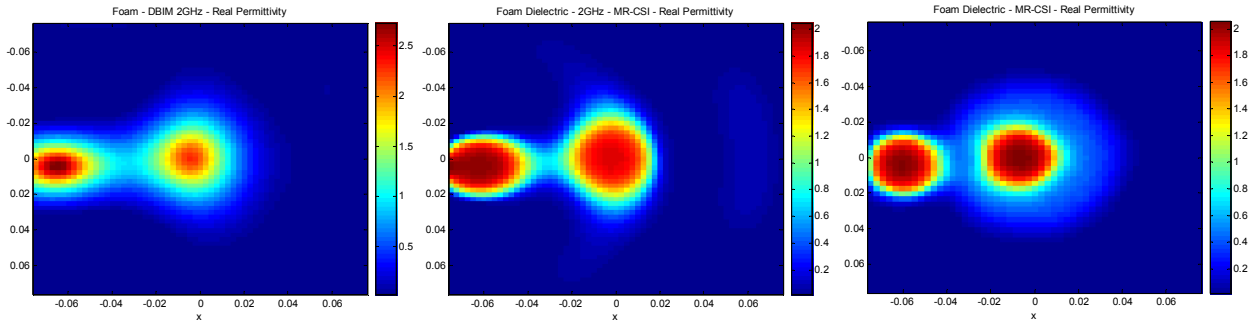

Fig. 2. Reconstructions of Fresnel data set *FoamTwinDielTM*. (a) DBIM reconstruction at 2 GHz, (b) MR-CSI reconstruction at 2 GHz, and (c) MR-CSI simultaneous, multi-frequency reconstruction using 2-10 GHz. The DBIM did not provide a meaningful reconstruction for the simultaneous multi-frequency inversion.